Structural and magnetoresistive properties of mechanically alloyed Fe-Co-Ag

Structural and magnetoresistive properties of mechanically alloyed Fe–Co–Ag

Neil S Cohen†‡, Quentin A Pankhurst† and Luis Fernández Barquín§

† Department of Physics and Astronomy, University College London, Gower Street,
London WC1E 6BT, UK
‡ Department of Chemistry, Birkbeck College, Gordon Street, London WC1H 0AJ, UK
§ Departamento CITIMAC, Facultad de Ciencias, Universidad de Cantabria, Santander 39005,
Spain

Abstract. The structural, magnetic and magnetoresistive properties of a wide range of mechanically alloyed Fe–Co–Ag granular materials were investigated by means of x-ray diffraction, Mössbauer spectroscopy, differential scanning calorimetry, DC magnetometry and magneto-resistance measurements. Binary Fe–Co alloys, milled using Syalon containers, showed a mixed fcc–bcc structure for Fe compositions between 20 and 25 at.%. The ternary alloys were found to comprise dispersions of Fe–Co grains in an fcc silver matrix, with the structure and magnetic properties of the Fe–Co grains mirroring those of the corresponding binary Fe–Co alloys. For materials with Fe:Co ratios in the region of the mixed fcc–bcc phases, additional components were noted in their Mössbauer spectra (a secondary sextet and a paramagnetic doublet, accounting for up to 63% of the spectral area), indicating the intermixing of a significant number of small Fe–Co clusters or fine grains into the Ag matrix. Alloys in this region were also found to have the largest magnetoresistive responses, with the maximum being a 5.8% effect in $(Fe_{0.15}Co_{0.85})_{30}Ag_{70}$, as measured at 10 K in a field of 3 T. This indicates the dominant significance of fine grain intermixing in these alloys.

1. Introduction

In the last decade there has been a resurgence of interest in heterogeneous granular alloys, especially those comprising small magnetic grains embedded in a non-magnetic metal matrix [1, 2]. The main impetus for this has been the potential for technological advances, such as the use of nanocrystalline alloys for soft magnetic applications, and granular alloys for sensor and read head applications. Examples of the latter include Co–Ag [3, 4], Fe–Ag [5, 6] and Fe–Co–Ag [7–10] granular alloys prepared by a variety of methods such as sputtering, co-evaporation, ion implantation, melt spinning, sol–gel synthesis and mechanical alloying. These materials show giant magnetoresistance (GMR) due to the formation of dispersed nanometre scale Fe, Co or Fe–Co alloy grains in the Ag matrix, and the resultant high volume density of interfacial scattering sites.

The functional properties of these alloys are intimately related to their microstructure. It is therefore valuable to establish which microstructures are accessible for a given set of preparation conditions, and relate them to the potentially useful properties of the system. Although such research is often conducted for one or two selected samples, it is uncommon for this to be carried through to a complete survey of a ternary alloy system. In response to this, we present here the results of a comprehensive study of the structural and magnetic

properties of the ternary system Fe–Co–Ag, as prepared by high-energy mechanical alloying. The preparation of materials by mechanical means is especially attractive for the formation of granular alloys, partly because of the large volumes and low costs of sample preparation compared to e.g. sputtering or melt spinning [11]. Another feature is that it is often found that metastable phases may be produced which are inaccessible by other preparation routes [11]. This latter point presents a second motivation for a survey of the Fe–Co–Ag system, which is to determine whether there are any hitherto unnoticed features of the phase diagram that might be of potential applied or fundamental interest.

In this paper we describe the results of a study of the structural, magnetic and magnetoresistive properties of the mechanically alloyed Fe–Co–Ag system, as determined via x-ray diffraction, EDAX analysis, DC magnetometry, ^{57}Fe Mössbauer spectroscopy and four-point magnetoresistance measurements. We show that the milled products contain dispersions of Fe–Co alloy grains in a granular silver matrix, with the Fe–Co adopting either an fcc or a bcc structure, dependent on composition and milling conditions. By first conducting a systematic investigation of the properties of the Fe–Co binary system, in particular using Mössbauer spectroscopy, we are able to unambiguously characterize the state of the Fe–Co grains in the Fe–Co–Ag ternary alloys. We show that the material which exhibits the maximum GMR signal is a granular alloy of composition $(Fe_{0.15}Co_{0.85})_{30}Ag_{70}$, and we relate this observation to the particular microstructure of this sample.

2. Experimental details

Thirty-eight different $(Fe_xCo_{1-x})_{1-y}Ag_y$ samples were prepared, with compositions chosen to systematically cover the ternary phase diagram (figure 1). The effect of composition on the alloy structure and the magnetoresistance was investigated for series of samples with the same x and varying Ag concentration, and for series of samples with the same y and varying Fe:Co ratios. Attention was also focused on the binary Fe–Co system, and on a region of high silver concentration for which significant GMR effects were found.
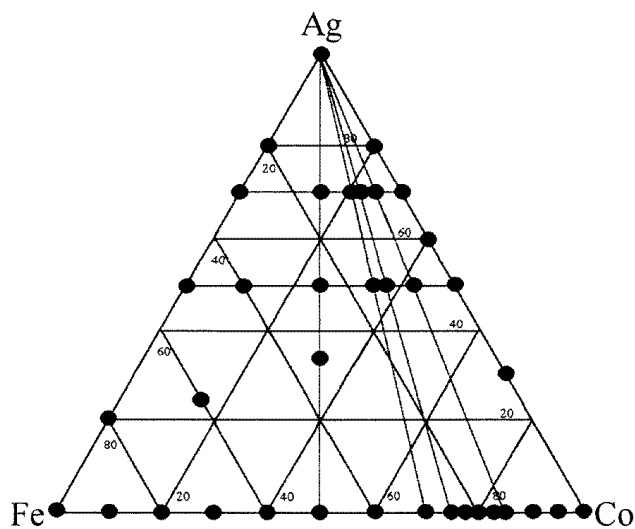

Figure 1. Fe–Co–Ag ternary phase diagram showing the sample compositions that were tested.

The milling was carried out using a Fritsch Pulverisette 7 high-energy planetary ball mill with either Syalon† or stainless steel‡ bowls and balls, operating at a disc rotation frequency of 600 rpm. Following an initial comparative study of a series of Fe–Co alloys milled using both Syalon and steel, a decision was taken to mill the remaining Fe–Co–Ag using the Syalon bowls and balls. Approximately 8 g of sample was used in each case, and the bowls were sealed in an inert argon atmosphere. To prevent excessive heating the mill was operated continuously for 2 hour periods, interspersed with cooling down periods of 1 hour. This limited the mill temperature to $40 \pm 5\,°C$. The maximum total milling time was typically 60 hours, but in some cases it was as much as 200 hours.

^{57}Fe Mössbauer spectra were collected using a constant acceleration unit in transmission geometry with an unpolarized 50 mCi source of ^{57}Co in an Rh matrix. A triangular drive waveform was used and the spectra were folded to remove any baseline curvature. Calibration was with respect to α-iron at room temperature. The spectra were analysed using a least squares fitting program based on a combination of standard methods, including Lorentzian doublets for the paramagnetic phases, and Voigtian sextets for the magnetic phases. The Voigtian profiles were constrained to have physically realistic and meaningful line positions and widths [12].

Structural analysis was carried out using a Philips X-Pert x-ray diffractometer in θ–θ reflection geometry with Mo Kα radiation ($\lambda = 0.7107$ Å). Differential scanning calorimetry (DSC) measurements were made using a Shimadzu DSC-50 operating from room temperature to 650 °C at a heating rate of 20 °C per minute. Samples of mass $\sim$20 mg were placed in open platinum pans, and the experiments were performed in a nitrogen atmosphere flowing at a rate of 20 ml min^{-1}. Impurity levels in the samples were measured via EDAX analysis. DC-magnetization measurements were made using a vibrating sample magnetometer in fields up to 0.75 T and temperatures from 77 K to 300 K. Magnetoresistance measurements were carried out on compressed pellets, using parallelepipeds of about 1 cm long and 3 mm^2 cross-section. Silver paste contacts were applied and values were obtained from a four-point probe resistometer in fields up to 3 T parallel to the direction of current flow, in the temperature range 10–300 K.

3. Binary iron–cobalt

3.1. Structure

The microstructures of the Fe–Co–Ag ternary alloys may be predicted from the properties of the three binary systems Fe–Ag, Co–Ag and Fe–Co. Both iron–silver and cobalt–silver are immiscible under equilibrium conditions, and remain largely immiscible even after prolonged ball milling [3, 4, 13]. In contrast, iron and cobalt are closely matched in atomic size, and alloy under equilibrium conditions, with a small negative heat of mixing of -1 kJ mol^{-1} [14]. They may be expected to be miscible by milling. The main difference between the elements is structural, with iron atoms forming a bcc lattice and cobalt an hcp/fcc lattice. Thus, in order for alloying to occur, a structural transformation is required on the part of one of the elements.

The anticipated structure of the ternary system is therefore that of Fe–Co alloy grains in a silver matrix, with the lattice structure of the grains to be determined. In order that we might be able to anticipate and compare the characteristics of the ternary alloys relative to the binary alloys, an initial study of the Fe–Co system was undertaken.

Two series of samples were made, one with the Syalon mill, and one with the stainless steel mill. These two materials have different densities, 3.2×10^3 kg m^{-3} for Syalon compared

---

† Predominantly Si$_3$N$_4$ with small amounts of yttrium and aluminium oxides incorporated.
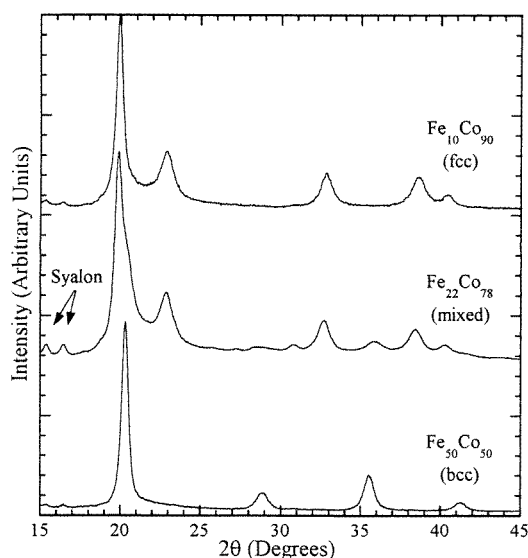‡ Type 4301 stainless steel: 68 at.% Fe, 19 at.% Cr, 8 at.% Ni, 2 at.% Si and traces of S and C.

Figure 2. X-ray diffraction patterns of selected Fe–Co alloys milled in Syalon containers, showing the change in structure with composition.

with 7.9×10^3 kg m^{-3} for stainless steel, which influences the impact energies during milling and thus the structure of the final product. The density also affects the ball-to-powder mass ratio, with 5:1 for Syalon compared to 12:1 for steel.

X-ray diffraction data on the Syalon milled samples showed that for Fe concentrations up to 20 at.% the lattice had an fcc structure, and for Fe concentrations above 25 at.% the lattice was bcc. A mixture of fcc and bcc phases formed for iron concentrations between 20 and 25 at.%, for which it was impossible to form a single phase alloy, even at extended milling times of up to 200 hours. Representative x-ray scans of these states are shown in figure 2. These results are similar to those found for Fe–Co alloys prepared from the melt, where a mixed phase region has been reported for Fe contents between 10 and 25 at.% [15, 16].

In some cases, an impurity component due to admixed Syalon particles was observed both in the x-ray data and in EDAX analyses. The most extreme example was a 7.8 at.% silicon content found after milling pure iron for 60 hours. Such impurities are inevitable given wear on the milling bowls and balls. However, these impurities were evidently immiscible with the sample material, given the separate phases found in the XRD patterns, and are therefore not likely to affect the sample properties.

It was noted that, although the ratio of bcc to fcc material fluctuated during milling, it ultimately settled at values related to the proximity of the pure bcc or fcc compositions. For example, $Fe_{22}Co_{78}$, which is close to the fcc region, contained a larger proportion of fcc material than did $Fe_{25}Co_{75}$. It was also noted that the required milling times for single phase alloying increased substantially on approaching the compositions of the mixed phase. For example, $Fe_{18}Co_{82}$ took 70 hours to complete the formation of an fcc alloy, and $Fe_{20}Co_{80}$ took 120 hours, rather than the more usual 20 hours. This observation is consistent with an increase in the enthalpy of formation for the alloy as the composition tends towards the critical values. Once the iron concentration rises above 20 at.% or falls below 25 at.%, the energy required becomes greater than that available from the milling process.

X-ray data for the stainless steel milled samples showed that the mixed phase region was no longer apparent, with the bcc region now extending down to an iron concentration of 10 at.%,
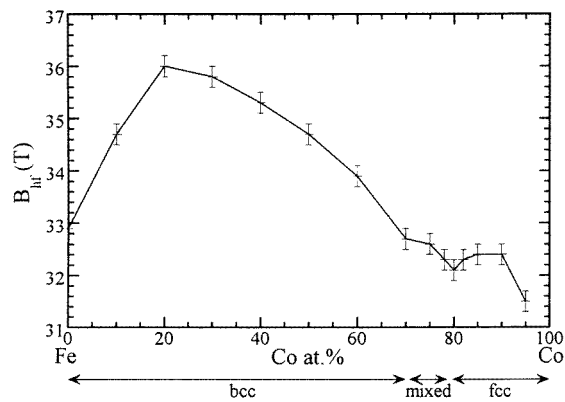
Figure 3. Plot showing the variation in Mössbauer hyperfine field with composition for Fe–Co samples milled for 60 hours in Syalon. The lattice structure of the resulting alloy is also marked.

and the remaining samples being fcc. This may be understood in terms of the increased milling energy afforded by the steel mill. Within what would otherwise be a mixed phase region, a *metastable* single phase alloy can form as a result of the extra energy imparted by the milling process. It was noted that the enthalpy of formation was again measurably greater in the 20–25 at.% Fe region, with samples such as $Fe_{90}Co_{10}$ requiring 20 hours rather than 10 hours milling. However, the alloying times in steel were generally half those in Syalon, e.g. 10 hours rather than 20 hours in the case of $Fe_{50}Co_{50}$.

Some impurities due to wear from the steel mill were found in the alloys, with typical Fe additions of order 3 at.% after 10 hours milling. While this in itself is not too significant an effect, we know from earlier studies that the chromium impurities, which are also incorporated into the samples, have a disproportionate effect, especially with regard to distortions in the Mössbauer data [13]. To avoid this complication, we decided to use the Syalon containers in preference to stainless steel for the remainder of the study.

3.2. Magnetic properties

The magnetic properties of Syalon-milled Fe–Co samples were investigated using both Mössbauer spectroscopy and DC magnetometry. The mean hyperfine fields B_{hf} of the samples showed a systematic variation over the composition range, shown in figure 3, reaching a maximum of 36.0 T for the bcc $Fe_{80}Co_{20}$ alloy. This is significantly larger than both pure bcc Fe ($B_{hf} = 33.0$ T) and fcc $Fe_{15}Co_{85}$ ($B_{hf} = 32.4$ T). This variation in hyperfine field is a manifestation of the well known Slater–Pauling curve [17] and has previously been observed in Fe–Co alloys made by both standard arc melting techniques [18] and by mechanical alloying [19]. The maximum in the curve is the point at which there is the greatest imbalance between spin up and spin down electrons in the 3d band, leading to the largest mean magnetic moment per atom. The Slater–Pauling curve is exactly mirrored by the Mössbauer hyperfine field, because the density of unpaired 3d conduction electrons affects the spin density of the core s electrons at the nucleus, which in turn gives rise to B_{hf} via the Fermi contact interaction [18].

DC magnetization measurements in fields of up to 0.75 T gave values for the maximum magnetization (σ_{max}) which also varied with sample composition as expected from the Slater–Pauling curve, although the absolute values were on average 10–20% lower than found
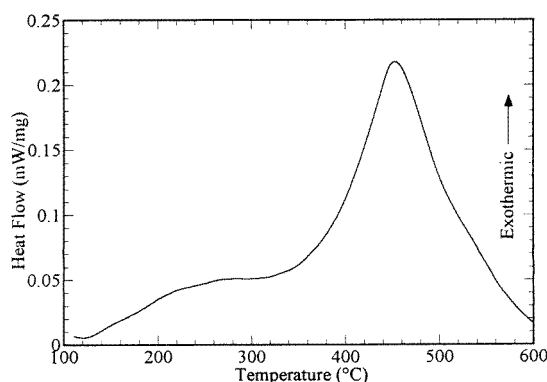
Figure 4. DSC curve for $Fe_{15}Co_{85}$ milled for 60 hours in Syalon.

in bulk alloys [17]. This may be due in part to the non-magnetic Syalon impurities in the ball-milled samples, but this is unlikely to account for all the difference. Another contribution could be related to the granular nature of the samples, since it has been reported that reduced magnetizations may be associated with magnetic atoms situated at grain boundaries rather than in the standard bulk environment [14].

3.3. Thermal properties

The Fe–Co alloys are known to be stable up to the respective melting points of the elements at around 1500 °C [15]. However, the alloys formed during ball milling differ from those produced under equilibrium conditions in that they consist of small, highly strained crystallites. Thermal treatment promotes lattice recovery and recrystallization processes. This is confirmed by the presence of exothermic peaks in the DSC measurements, an example of which is shown, for $Fe_{15}Co_{85}$, in figure 4. The behaviour is similar to that seen for milled pure iron [20]. Since both iron and cobalt have similarly high melting points, the alloy lattice is able to store substantial energy during milling, in this case 9 kJ mol^{-1}, which is then gradually released on heating to 600 °C. The most intense exotherm is in the 400–500 °C range, which is a region previously identified as one in which recrystallization processes occur [20].

　　The effects of thermal treatment were further explored by recording the Mössbauer spectra of aliquots of a sample of $Fe_{70}Co_{30}$ before and after heating (see figure 5). This composition was chosen as it lies at the peak of the Slater–Pauling curve and thus has a hyperfine field that is visibly different from that of standard α-Fe. It can be seen in figure 5 that on heating the hyperfine field of the main sextet remains constant, and there is no sign of a separate α-Fe component appearing. This demonstrates that the Fe–Co alloy remains stable and there is no phase segregation. The linewidth also remains broad, not because of structural disorder but because the alloy is a random substitutional solid solution. The iron atoms thus have different arrangements of iron and cobalt nearest neighbours, which results in a distribution of B_{hf} values. The structural changes on heating are evident from the decrease in area of the second magnetic component, which was modelled to take into account the presence of iron atoms in a non-cubic environment. These could be atoms at grain boundaries or distorted lattice sites, but in either case the heating process can be seen to reduce their number due to the recrystallization and grain growth processes.
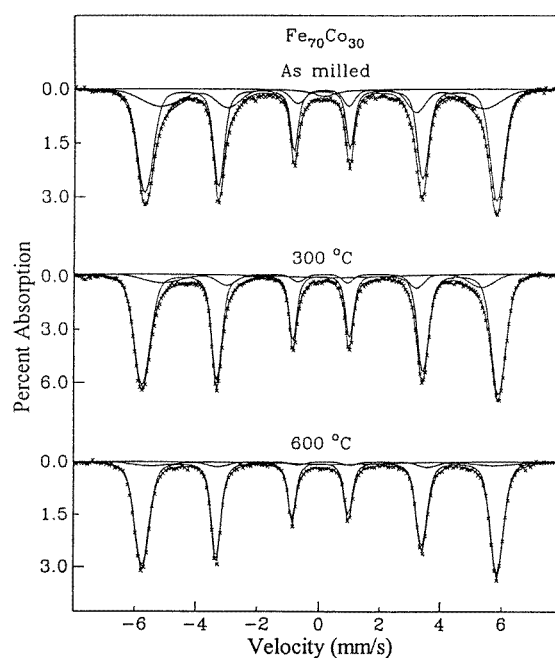
Figure 5. Mössbauer spectra of the $Fe_{70}Co_{30}$ alloy, as milled and after heating in the DSC to 300 and 600 °C. The solid lines are least-squares fits to the data, as discussed in the text.

4. Ternary iron–cobalt–silver

4.1. Structure

Figure 6 shows x-ray patterns for selected samples from the $(Fe_xCo_{1-x})_{50}Ag_{50}$ series. It is clear that the majority of silver atoms remain in an unalloyed fcc state, with the Ag(111) peak clearly visible. From this peak width, using the Scherrer formula, the Ag particle sizes were estimated as ~120 Å. There is also evidence that Fe–Co alloy grains have been formed, with structures largely the same as in the binary Fe–Co alloys. In those materials with a low Fe:Co ratio, such as the $(Fe_{0.15}Co_{0.85})_{50}Ag_{50}$ shown in figure 6, a distinct fcc-Fe–Co structure is visible in the XRD pattern. Those samples with an Fe:Co ratio of 25:75 and above, for which this feature is absent, presumably contain bcc magnetic grains. However, it is not possible to visually separate the diffraction pattern of bcc Fe–Co from the fcc pattern of silver due to the similarity in peak positions.

Further evidence for the granular structure comes from the Mössbauer spectra shown in figures 7 and 8. If separate magnetic Fe–Co grains exist in the ternary $(Fe_xCo_{1-x})_{1-y}Ag_y$ sample, the main Mössbauer sextet should have the same hyperfine parameters as the binary Fe_xCo_{1-x} alloy on which the ternary material is based, as distinct from α-Fe. It can be seen from the data in table 1 that this similarity in hyperfine parameters does indeed occur, and it can be confirmed that the bulk structure is of the granular Fe–Co plus Ag type.

The Mössbauer spectra of figures 7 and 8 show some interesting additional features. Each spectrum was fitted with three components; two ferromagnetic sextets and one paramagnetic doublet. The main, sharp sextet is that of the bulk Fe–Co particles as described above, and the second sextet is due to iron atoms at grain boundaries and surfaces, which are in a non-standard
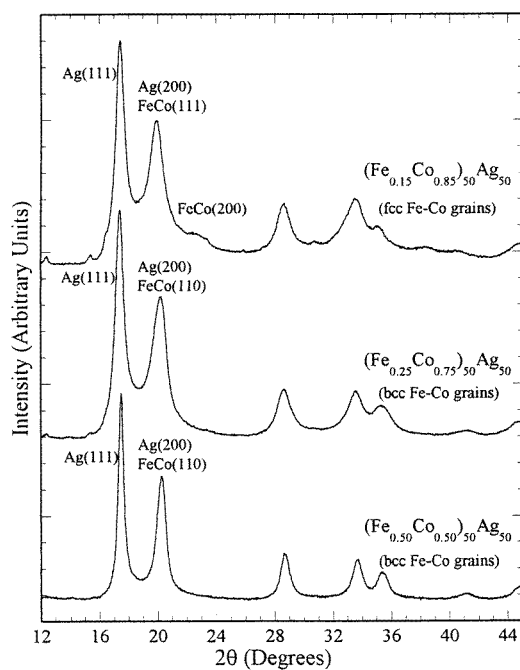
Figure 6. X-ray diffraction patterns of selected samples from the $(Fe_xCo_{1-x})_{50}Ag_{50}$ series, showing the varying structure of the magnetic grains.
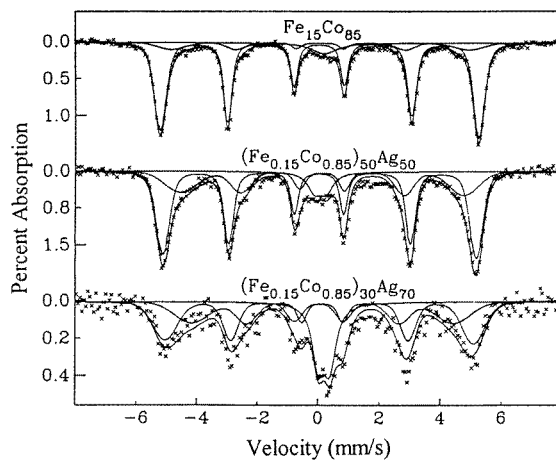

Figure 7. Mössbauer spectra of selected samples from the $(Fe_{0.15}Co_{0.85})_{1-y}Ag_y$ series. The solid lines are least-squares fits to the data, as discussed in the text.

environment. The third, paramagnetic doublet results from iron atoms (or extremely small Fe–Co clusters, of a few atoms only) that are alloyed or otherwise dispersed within the fcc silver matrix. This doublet indicates that while the silver is largely immiscible with the Fe–Co grains, there is a limited amount of solid solubility. This is not unexpected given the non-equilibrium nature of the mechanical alloying process. Similar results have been seen in ball-milled Fe–Ag [21], in which 10 at.% of the iron was found to be in a paramagnetic phase.
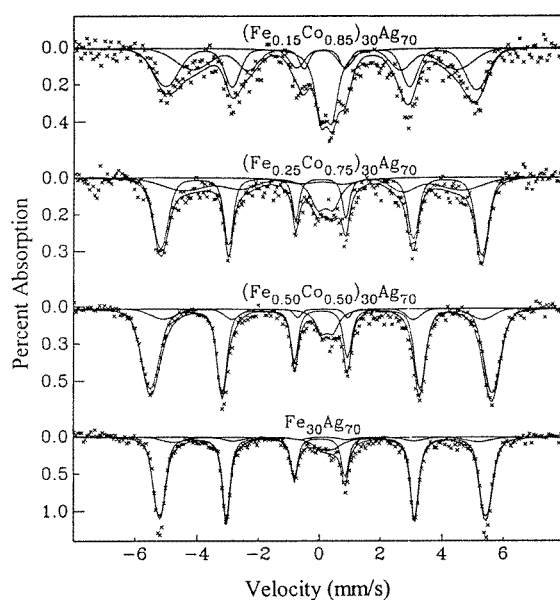
Figure 8. Mössbauer spectra of selected samples from the $(Fe_x Co_{1-x})_{30} Ag_{70}$ series. The solid lines are least-squares fits to the data, as discussed in the text.

Furthermore, using vapour quenching methods such as RF sputtering, where it is possible to produce structures even further from equilibrium, complete single phase $Fe_{1-x} Ag_x$ alloys have been synthesized [22]. These were of a bcc structure for $x \leqslant 14$ and fcc for $x \geqslant 60$, for which the characteristic Mössbauer signal was a quadrupole split doublet.

Figure 7 also shows that both the secondary sextet and the doublet increase in relative area with the proportion of silver in the sample. This is reasonable, given that with a fixed percentage solubility of the magnetic material in silver, but an increased silver concentration, more iron atoms should enter the fcc-Ag lattice, hence increasing the doublet area. Similarly, an increase in silver concentration should lead to a greater likelihood of interfacial mixing at grain boundaries, thus increasing the area of the secondary sextet.

Figure 8 shows that the relative areas of the secondary sextet and the doublet decrease as the Fe:Co ratio increases. This apparent fall in miscibility suggests that while both iron and cobalt are largely immiscible in silver, cobalt is marginally less so. Given the otherwise similar nature of cobalt and iron in terms of atomic size and electronic properties, this may be explained by the fact that cobalt favours an fcc lattice arrangement, like that of silver, whereas iron usually exists in a bcc structure. This adds weight to the hypothesis that the secondary sextet and doublet relate to clusters of a few iron and cobalt atoms, in an fcc arrangement, alloyed with the silver, rather than isolated atoms in a true substitutional solid solution.

4.2. Thermal properties

To obtain further evidence on the degree and nature of the alloying in the ternary system, DSC experiments were performed on selected samples. The DSC curves showed broad exothermic peaks similar to those previously seen for the Fe–Co alloys. More informative, however, were Mössbauer spectra recorded on the DSC residues, after heating to 600 °C, one of which is shown in figure 9 for the $(Fe_{0.15} Co_{0.85})_{30} Ag_{70}$ sample. The main sextet in the spectrum of

Table 1. Mössbauer data for the ternary Fe–Co–Ag system, milled in Syalon containers. The hyperfine parameters of the related binary Fe–Co samples (main components only) are included for comparison. Also tabulated is the room temperature resistivity of the sample pellets, and their magnetoresistance measured 10 K in a 3 T field.

Sample	δ (mm s^{-1})	Δ (mm s^{-1})	B_{hf} (T)	ΔB_{hf} (T)	Area	ρ ($\times 10^{-8}$ Ω m)	MR (%)
Co$_{30}$Ag$_{70}$						65(2)	4.8(2)
(Fe$_{0.15}$Co$_{0.85}$)$_{30}$Ag$_{70}$	0.02(1)	—	31.3(2)	1.7(5)	0.37(4)	50(2)	5.8(2)
	0.15(2)	—	26.8(7)	2.5(12)	0.26(4)		
	0.21(1)	0.38(2)	—	—	0.37(4)		
(Fe$_{0.15}$Co$_{0.85}$)$_{50}$Ag$_{50}$	0.03(1)	—	32.0(2)	1.3(3)	0.59(4)	42(2)	2.4(2)
	0.13(2)	—	28.9(5)	2.3(8)	0.32(4)		
	0.08(2)	0.40(3)	—	—	0.08(3)		
Fe$_{15}$Co$_{85}$	0.02(1)	—	32.4(1)	1.2(1)			
(Fe$_{0.25}$Co$_{0.75}$)$_{30}$Ag$_{70}$	0.02(1)	—	32.4(1)	1.4(4)	0.58(3)	80(2)	5.7(2)
	0.06(6)	—	28.3(6)	2.5(10)	0.28(4)		
	0.18(4)	0.50(5)	—	—	0.14(3)		
(Fe$_{0.25}$Co$_{0.75}$)$_{50}$Ag$_{50}$	0.03(2)	—	32.7(2)	1.4(3)	0.64(3)		
	0.05(3)	—	27.3(4)	3.1(9)	0.22(3)		
	0.12(3)	0.45(5)	—	—	0.15(3)		
Fe$_{25}$Co$_{75}$	0.03(1)	—	32.6(1)	1.4(4)			
(Fe$_{0.30}$Co$_{0.70}$)$_{30}$Ag$_{70}$	0.02(1)	—	32.3(1)	1.3(4)	0.47(3)	65(2)	5.5(2)
	0.12(2)	—	27.8(6)	2.2(15)	0.19(3)		
	0.23(1)	0.43(2)	—	—	0.35(3)		
(Fe$_{0.30}$Co$_{0.70}$)$_{50}$Ag$_{50}$	0.02(1)	—	33.0(1)	1.3(3)	0.75(3)		
	0.07(2)	—	29.9(4)	2.4(8)	0.20(2)		
	0.10(2)	0.41(4)	—	—	0.05(2)		
Fe$_{30}$Co$_{70}$	0.03(1)	—	32.8(1)	0.5(2)			
(Fe$_{0.50}$Co$_{0.50}$)$_{30}$Ag$_{70}$	0.05(1)	—	34.7(2)	1.0(3)	0.77(3)	72(2)	1.6(2)
	0.10(2)	—	32.0(5)	2.0(7)	0.14(2)		
	0.25(3)	0.38(5)	—	—	0.09(2)		
(Fe$_{0.50}$Co$_{0.50}$)$_{50}$Ag$_{50}$	0.04(1)	—	34.3(1)	1.6(5)	0.74(3)		
	0.14(2)	—	32.1(3)	2.3(9)	0.17(2)		
	0.27(2)	0.50(4)	—	—	0.08(2)		
(Fe$_{0.50}$Co$_{0.50}$)$_{67}$Ag$_{33}$ [a]	0.05(1)	—	34.8(2)	1.6(7)	0.53(4)		
	0.05(1)	—	32.0(5)	2.1(7)	0.43(4)		
	0.10(4)	0.50(5)	—	—	0.03(2)		
Fe$_{50}$Co$_{50}$	0.03(1)	—	34.7(1)	1.6(3)			
(Fe$_{0.80}$Co$_{0.20}$)$_{50}$Ag$_{50}$ [a]	0.04(1)	—	36.1(1)	0.5(3)	0.70(3)		
	0.10(1)	—	32.3(5)	1.1(4)	0.18(2)		
	0.33(2)	0.66(3)	—	—	0.11(2)		
(Fe$_{0.80}$Co$_{0.20}$)$_{75}$Ag$_{25}$ [a]	0.04(1)	—	35.7(2)	1.3(4)	0.58(3)		
	0.05(1)	—	32.7(5)	2.1(6)	0.38(3)		
	0.19(2)	0.34(2)	—	—	0.04(2)		
Fe$_{80}$Co$_{20}$	0.04(1)	—	36.0(1)	0.6(2)			
Fe$_{20}$Ag$_{80}$	0.01(1)	—	33.2(1)	0.8(4)	0.54(3)		
	0.08(2)	—	31.9(3)	2.0(5)	0.15(3)		
	0.26(2)	0 (fixed)	—	—	0.31(5)		
Fe$_{30}$Ag$_{70}$	0.01(1)	—	33.0(1)	0.5(3)	0.82(2)	32(2)	1.8(2)
	0.11(2)	—	31.3(3)	2.2(12)	0.09(2)		
	0.26(2)	0.40(5)	—	—	0.08(2)		
Fe$_{50}$Ag$_{50}$	0.01(1)	—	33.0(1)	1.1(2)	0.71(2)		
	0.08(1)	—	30.8(4)	2.4(7)	0.23(2)		
	0.24(2)	0 (fixed)	—	—	0.05(2)		

[a] Samples milled in steel.
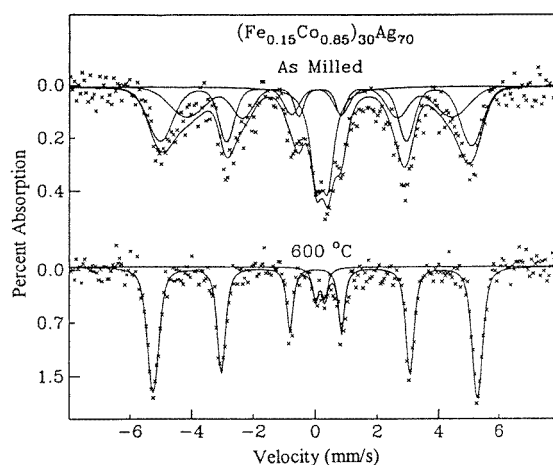
Figure 9. Mössbauer spectra of $(Fe_{0.15}Co_{0.85})_{30}Ag_{70}$, as milled and after heating to 600 °C. The solid lines are least-squares fits to the data, as discussed in the text.

the residue has a mean hyperfine field $B_{hf} = 32.7 \pm 0.1$ T and a Gaussian spread in fields $\Delta B_{hf} = 1.5 \pm 0.1$ T. These parameters are similar to those observed for the binary $Fe_{15}Co_{85}$ and $Fe_{25}Co_{75}$ alloys, implying that the residue contains Fe–Co alloy grains, with little or no separation into distinct iron and cobalt phases. Additionally, the broad sextet in the as-made sample disappeared and the doublet was substantially reduced in area. This can be taken as evidence for the decomposition of any partially alloyed Fe–Co–Ag crystallites, which is to be expected given their metastable nature.

4.3. Magnetic properties

The M_{DC} measurements confirmed the existence of Fe–Co grains in a silver matrix, since the observed maximum magnetization values vary with composition along the Slater–Pauling curve, as did the Mössbauer hyperfine field parameters. They also showed that the bulk of the particles behaved as ferromagnetic rather than superparamagnetic grains, something that has been seen in similar ball-milled material [3, 4, 23]. The critical volume, below which super-paramagnetic behaviour is expected, has been calculated for cobalt grains to be 8×10^4 Å^3 [23], corresponding to a grain diameter of 54 Å. This value is less than the mean grain size of the ball-milled Fe–Co–Ag samples, which was estimated as 60–80 Å from x-ray line broadening. Thus ferromagnetic behaviour is to be expected. However, given a broad distribution in particle sizes, it is possible that a superparamagnetic component exists, albeit masked by the ferromagnetic response of the larger grains [23, 24].

4.4. Magnetoresistance: dependence on composition and microstructure

Magnetoresistance (MR) measurements were made on selected samples in fields of up to 3 T, at 10 K, with the results shown in figure 10 and summarized in table 1. Most of the resistivity change occurs within a 1 T field. It was found that the MR in the $(Fe_xCo_{1-x})_{30}Ag_{70}$ sample series was consistently higher than in the $(Fe_xCo_{1-x})_{50}Ag_{50}$ series. For example, $(Fe_{0.15}Co_{0.85})_{30}Ag_{70}$ had a maximum MR of 5.8%, while the MR of $(Fe_{0.15}Co_{0.85})_{50}Ag_{50}$ was only 2.4%. This is in accordance with theoretical predictions of maximum MR for a metal

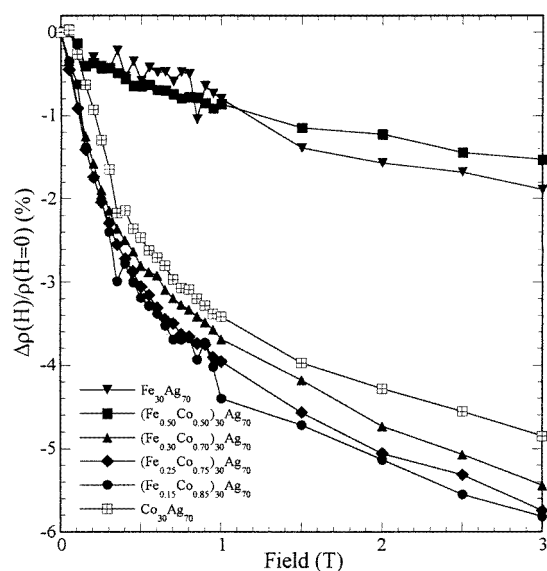**Figure 10.** Magnetoresistance measurements at 10 K for the $(Fe_xCo_{1-x})_{30}Ag_{70}$ series. Magnetoresistance is given by $\Delta\rho(H)/\rho(H=0)$ where $\Delta\rho(H) = \rho(H=0) - \rho(H)$.

volume fraction of $\sim$25% [25] and with experimental results from similar granular materials where the highest MR values were found in samples with a metal volume fraction of 19–28% [26, 27]. Higher concentrations of magnetic material lead to the formation of extended multi-domain ferromagnetic regions as the separate magnetic grains interact and coalesce, and a consequent reduction in magnetoresistance. Consequently, we focused our attention on the $(Fe_xCo_{1-x})_{30}Ag_{70}$ sample series.

The absolute resistivities of the selected samples, listed in table 1, are relatively high, with $\rho \sim 60 \times 10^{-8}$ Ω m, compared to those reported in sputtered GMR films, where ρ is usually in the range $10–30 \times 10^{-8}$ Ω m [24]. The origin of this high residual resistivity lies in the fact that the samples comprise coarse particles that are difficult to compact. The pressed pellets are therefore relatively porous, despite being subjected to a pressure of 230 MPa. We note that the measured residual resistivities for the pellets (table 1) range from 32 to 80×10^{-8} Ω m, which variation we suspect is largely due to differences in the effectiveness of the sample compaction in each case. If these data were normalized to the same ρ then the largest GMR would appear in $(Fe_{0.25}Co_{0.75})_{30}Ag_{70}$. We also note that the percentage magnetoresistance values would all be significantly higher if there were a lower residual resistance. Using the same measured value of $\Delta\rho \sim 3 \times 10^{-8}$ Ωm, but with values of ρ similar to those obtained in films, the resulting GMR values would be closer to 20% than the 3–6% measured. It is therefore probable that significant improvements in the GMR properties might be achieved by optimizing the sample compaction technology, perhaps combined with thermal treatments.

It is notable that the magnetoresistance is maximized for materials in the region around $(Fe_{0.20}Co_{0.80})_{30}Ag_{70}$, where the Fe:Co ratio lies in the mixed phase region found for the binary Fe–Co alloys. This implies that the sample microstructure plays a role in determining the MR response. One factor to consider in this context is the differential alloying behaviour highlighted by the Mössbauer spectra. The doublet component, which indicates the presence of small or partially alloyed clusters or grains, is most prominent in the samples with the largest MR, accounting for 37% of the spectral area for the $(Fe_{0.15}Co_{0.85})_{30}Ag_{70}$ sample.
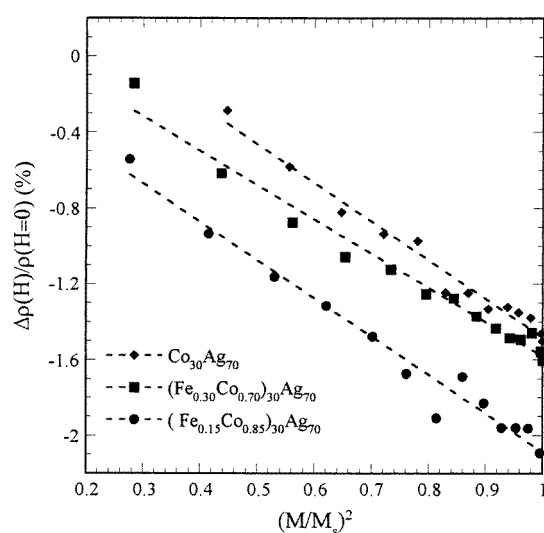
Figure 11. Relative variation of magnetoresistance ($\Delta\rho(H)/\rho(H = 0)$ where $\Delta\rho(H) = \rho(H = 0) - \rho(H)$) as a function of the quadratic variation of magnetization $(M/M_S)^2$ for selected samples at 300 K. The variation is rather linear confirming the expected correlation between the magnetoresistance of the magnetization, through the spatial correlation between moments of different particles. Deviations from this linear behaviour can arise from distribution of sizes in the particles (see text).

This contrasts with only a 9% doublet area in the $(Fe_{0.50}Co_{0.50})_{30}Ag_{70}$ sample, and no doublet at all in the $Fe_{30}Ag_{70}$ sample, both of which had poor MR responses. The clear implication is that an increase in the amount of small clusters or grains can enhance the MR properties.

An associated factor which could lead to enhanced MR for samples with compositions in the Fe–Co mixed phase region is the enthalpic competition between the fcc and bcc structures in the Fe–Co grains. This may be expected to promote the formation of small Fe–Co clusters and grains embedded in the fcc Ag matrix, with correspondingly high interfacial area to volume ratios, and larger MR.

An interesting question is whether the intrinsic crystal structures of the Fe–Co grains affect the MR. It has been reported for Fe–Co/Cu multilayers that larger MR values can be obtained when the iron and cobalt atoms are alloyed in an fcc lattice, and that there is a sharp decrease in MR as the Fe:Co ratio increases beyond the fcc–bcc transition point [28]. However, in thin film granular Fe–Co–Ag samples a similar observation was explained by changes in grain size alone [29]. The present mechanically alloyed samples appear to fall into the latter category. The alloys $(Fe_{0.15}Co_{0.85})_{30}Ag_{70}$, $(Fe_{0.25}Co_{0.75})_{30}Ag_{70}$ and $(Fe_{0.30}Co_{0.70})_{30}Ag_{70}$ have Fe:Co ratios that place them in the fcc, mixed fcc–bcc and bcc regions of the Fe–Co phase diagram respectively; but all three samples have MR values of the order of 6%. There is also no dramatic difference in the mixing between the magnetic and non-magnetic grains in these samples, as evidenced by their similar Mössbauer spectra.

4.5. Magnetoresistance: analysis of MR curves

The magnetoresistive $\rho(H)$ behaviour is mainly driven by spin dependent scattering as the electrons are successively scattered by the magnetic grains. In this way, it is well known

that $\Delta\rho/\rho \propto M^2$ as a result of the statistical average of the magnetization angle between neighbouring non-interacting particles, which depends explicitly depending on $\langle\cos(\theta_i - \theta_j)\rangle$, where θ is the angle of the magnetization of each grain relative to the direction of electron transport [30]. Figure 11 shows a plot of $\Delta\rho/\rho$ as a function of $(M/M_s)^2$ at room temperature for three of the mechanically alloyed Fe–Co–Ag samples. The purely quadratic dependence is obeyed in general terms in those materials that also showed the larger MR values, more than 4% (at 10 K and 3 T). Small deviations from this behaviour have recently been proposed, based on studies of (CoFe)–Cu ball-milled and NiFe–Ag sputtered alloys in which a portion of particles are thought to exist in a superparamagnetic state and two different contributions are used, their validity depending on the $(M/M_s)^2$ range [31, 32]. In our case this more complex behaviour cannot be conclusively found, as more data points corresponding to low-field $(M/M_s)^2$ values would be needed.

5. Conclusions

The structural, magnetic and magnetoresistive properties of the mechanically alloyed Fe–Co–Ag system were investigated. A full study of the ternary phase diagram was undertaken. It was found to be possible to produce materials comprising Fe–Co alloy particles embedded in a silver matrix, some of which showed GMR effects.

In the binary Fe–Co system milling was carried out using both Syalon and steel containers, with the lattice structure and Mössbauer hyperfine parameters measured as a function of composition. The samples milled in Syalon had a bcc structure if the iron concentration was >25 at.%, an fcc structure when it was <20 at.% and a mixed fcc–bcc structure between those values. In the steel-milled material the mixed phase region disappeared, to be replaced with an extended bcc zone.

Several series of ternary granular alloys were milled using the Syalon containers, resulting in nanocomposite materials comprising a dispersion of Fe–Co grains in a silver matrix. Comparison of the Mössbauer hyperfine field values in the $(Fe_xCo_{1-x})_{1-y}Ag_y$ system with those in equivalent Fe_xCo_{1-x} samples showed that similar Fe–Co particles were present in each case. Although the magnetic and non-magnetic grains were largely immiscible, it was seen from the presence of additional components in the Mössbauer spectra (a secondary sextet and a paramagnetic doublet) that there was a limited degree of alloying between them, particularly in those samples with cobalt rich magnetic particles.

Given the miscibility of iron and cobalt, no phase separation was seen on thermal treatment of the binary alloys at temperatures of up to 600 °C, although lattice recovery and recrystallization processes were visible. In the case of the ternary system, however, the limited alloying of the magnetic grains with the silver was removed during heating.

The magnetoresistance of some of the Co–Ag and Fe–Co–Ag systems was investigated, with the largest MR, 5.8% in 3 T at 10 K, being found in $(Fe_{0.15}Co_{0.85})_{30}Ag_{70}$. The measured MR values were smaller than might be achievable, due to the large residual resistivities of the pressed sample pellets, caused in part by porosity. The field dependent magnetoresistance was found to vary in proportion to M^2 behaviour for the compositions with large MR values, following expected behaviour for granular GMR systems.

The ball-milled Fe–Co–Ag alloys that had the largest MR were those with the highest proportion of small Fe–Co clusters or fine grain intermixing with the Ag matrix, as evidenced by secondary sextets and doublets in their Mössbauer spectra. This coincided with those materials whose Fe:Co ratios were close to those of the mixed fcc–bcc phase Fe–Co alloys, indicating that in this system the microstructure of the magnetic grains carries a decisive role in the formation of magnetoresistive materials.

Acknowledgments

References

[1] Hadjipanayis G C and Siegel R W 1994 *Nanophase Materials: Synthesis, Properties, Applications* (Dordrecht: Kluwer)
[2] Dormann J L and Fiorani D 1992 *Magnetic Properties of Fine Particles* (Amsterdam: North-Holland)
[3] Coey J M D, Fagan A J, Skomski R, Gregg J, Ounadjela K and Thompson S M 1994 *IEEE Trans. Magn.* **30** 666–8
[4] Thompson S M, Gregg J F, Staddon C R, Daniel D, Dawson S J, Ounadjela K, Hammann J, Fermon C, Saux G, O'Grady K, Grieves S J, Coey J M D and Fagan A J 1993 *Phil. Mag.* B **68** 923–37
[5] Wang J P, Luo H L, Gao N F and Liu Y Y 1996 *J. Mater. Sci.* **31** 727–30
[6] de Azevedo M M P, Sousa J B, Mendes J A, Almeida B G, Rogalski M S, Pogorelov Y G, Bibicu I, Redondo L M, da Silva M F, Jesus C M, Marques J G and Soares J C 1997 *J. Magn. Magn. Mater.* **173** 230–40
[7] Tsoukatos A, Dimitrov D V, Murthy A S and Hadjipanayis G C 1994 *J. Appl. Phys.* **76** 6799–801
[8] Tsoukatos A, Wan H, Hadjipanayis G C and Unruh K M 1993 *J. Appl. Phys.* **73** 5509–11
[9] Redon O, Pierre J, Rodmacq B, Mevel B and Dieny B 1995 *J. Magn. Magn. Mater.* **149** 398–408
[10] Cohen N S, Pankhurst Q A and Fernández Barquín L 1998 *Hyperfine Interact.* C **3** 285–8
[11] Campbell S J and Kaczmarek W A 1996 *Mössbauer Spectroscopy Applied to Magnetism and Magnetic Materials* vol 2 ed G J Long and F Grandjean (New York: Plenum) p 276–8
[12] Lines M E and Eibschütz M 1983 *Solid State Commun.* **45** 435–9
[13] Cohen N S, Ahlswede E, Wicks J D and Pankhurst Q A 1997 *J. Phys.: Condens. Matter* **9** 3259–76
[14] Kuhrt C and Schultz L 1992 *J. Appl. Phys.* **71** 1896–900
[15] Hansen M and Anderko K 1958 *Constitution of Binary Alloys* (New York: McGraw-Hill) pp 471–4
[16] Andrews M R 1921 *Phys. Rev.* **18** 245–54
[17] Jiles D 1991 *Introduction to Magnetism and Magnetic Materials* (London: Chapman and Hall) pp 263–8
[18] Johnson C E, Ridout M S and Cranshaw T E 1963 *Proc. Phys. Soc.* **81** 1079–90
[19] Brüning R, Samwer K, Kuhrt C and Schultz L 1992 *J. Appl. Phys.* **72** 2978–83
[20] Pankhurst Q A, Cohen N S and Odlyha M 1998 *J. Phys.: Condens. Matter* **10** 1665–76
[21] Kuyama J, Inui H, Imaoka S, Nasu S, Ishihara K N and Shingu P H 1991 *Japan J. Appl. Phys. Lett.* **30** L854–6
[22] Kataoka N, Sumiyama K and Nakamura Y, 1985 *J. Phys. F: Met. Phys.* **15** 1405–11
[23] Fagan A J, Viret M and Coey J M D 1995 *J. Phys.: Condens. Matter* **7** 8953–66
[24] Stearns M B and Cheng Y 1994 *J. Appl. Phys.* **75** 6894–9
[25] Chien C L, Xiao J Q and Jiang J S 1993 *J. Appl. Phys.* **73** 5303–14
[26] Berkowitz A E, Mitchell J R, Carey M J, Young A P, Zhang S, Spada F E, Parker F T, Hutten A and Thomas G 1992 *Phys. Rev. Lett.* **68** 3745–8
[27] Xiao J Q, Jiang J S and Chien C L 1992 *Phys. Rev. Lett.* **68** 3749–52
[28] Kano H, Iwasaki Y, Hayashi K and Aso K, 1993 *J. Magn. Magn. Mater.* **126** 445–7
[29] Kubinski D J and Holloway H 1995 *J. Appl. Phys.* **77** 2010–4
[30] Gittleman J I, Goldstein Y and Bozowski S 1972 *Phys. Rev.* B **5** 3609
[31] Nagamine L C C M, Chamberod A, Auric P, Auffret S and Chaffron L 1997 *J. Magn. Magn. Mater.* **174** 309–15
[32] Badia F, Battle X, Labarta A, Watson M L, Johnston A B and Chapman J N 1997 *J. Appl. Phys.* **82** 677–87